Advanced Ceramics Progress: Vol. 11, No. 1, (Winter 2025) 47-53

Materials and Energy Research Center
MERC

Contents lists available at ACERP

Advanced Ceramics Progress

Journal Homepage: www.acerp.ir

Original Research Article

Sonochemical Synthesis of Highly Uniform ZnO Nanoparticles on 3D Monolithic Cordierite Honeycomb Substrates

Seyed Salman Afghahi [a], Farshad Soleimani [b] *

[a] *Department of Materials Engineering, Faculty of Materials Engineering, Imam Hossein University, Tehran, Iran.*
[b] *Department of Materials Engineering, Facaulty of Engineering, Malayer University, Malayer, Hamedan, Iran.*

* Corresponding Author Email: f.soleimani@malayeru.ac.ir (F. Soleimani) URL: https://www.acerp.ir/article_234516.html

ARTICLE INFO

Article History:
Received 17 September 2025
Received in revised form 04 October 2025
Accepted 16 November 2025

Keywords:
Cordierite Honeycomb,
ZnO,
Nano Array,
Sonochemical

ABSTRACT

This study investigates the sonochemical deposition of ZnO nanoparticles onto a monolithic cordierite honeycomb substrate. The research systematically evaluated the impact of two key parameters, sonication power (100–400 W) and zinc acetate dihydrate concentration (10–40 mM). The successful formation of the ZnO phase on the cordierite support was confirmed through X-ray diffraction (XRD) and scanning electron microscopy (SEM) analyses. The crystallite size of the deposited ZnO nanoparticles was determined using both the Scherrer equation and Rietveld refinement methods applied to XRD data. The findings revealed that an increase in sonication power from 100 to 400 W, at a fixed zinc acetate concentration of 40 mM, resulted in a significant reduction of ZnO crystallite size. Furthermore, this higher power enhanced the uniformity of the nanoparticle coating on the honeycomb channels. A similar trend was observed with precursor concentration; increasing the zinc acetate concentration from 10 to 40 mM led to a further decrease in nanoparticle crystallite size. Based on these results, the study identifies the optimized synthesis conditions for achieving the most favorable nanoparticle characteristics. The sample prepared with a sonication power of 400 W and a zinc acetate concentration of 20 mM was determined to provide the optimal outcome.

https://doi.org/10.30501/acp.2025.547739.1184

1. INTRODUCTION

Zinc Oxide (ZnO) is an inorganic compound that usually appears as white powder, nearly insoluble in water. ZnO, with its unique physical and chemical properties, such as high chemical stability, high electrochemical coupling coefficient, broad radiation absorption range, and high photostability, is a multifunctional material. In materials science, ZnO is classified as a semiconductor in Group II-VI, whose covalence lies on the boundary between ionic and covalent semiconductors. A broad energy band (3.37 eV), high bond energy (60 meV), and high thermal and mechanical stability at room temperature make it attractive for potential use in UV-light emitters (X. Ren et al., 2015), varistors (Maleki Shahraki et al., 2011), surface acoustic wave devices (Magnusson et al., 2015), piezo-electric transducers (Yanagitani et al., 2011), gas sensors (Kang et al., 2021), catalysts (Guo et al., 2013), and biosensors (Zhu et al., 2016). Various ZnO nanostructures such as nanoparticles, nanorods, nanocombs, nanorings, nanohelices, nanosprings, nanobelts, nanowires, and nanocages were already developed (Liu et al., 2010; Safaee et al., 2015; Wang, 2004). For catalytic applications, a high surface area and proper arrangement of nanostructures are important. Although various nanostructures such as nanoparticles and nanowire-based powder-form catalysts have shown promising potential as efficient catalysts (Xie et al., 2009; Yang et al., 2008), nanostructure-based monolithic catalysts have been rarely investigated due to the lack of

Please cite this article as: Afghahi, S. S. & Soleimani, F. (2025). Sonochemical Synthesis of Highly Uniform ZnO Nanoparticles on 3D Monolithic Cordierite Honeycomb Substrates, *Advanced Ceramics Progress*, 11(1), 47-53. https://doi.org/10.30501/acp.2025.547739.1184

2423-7485/© 2025 The Author(s). Published by MERC.
This is an open access article under the CC BY license (https://creativecommons.org/licenses/by/4.0/).

an effective integration strategy. Monolithic cordierite honeycomb with hundreds of channels is extensively known as a three-dimensional support for different energy and environmental catalysts and is predominantly used in both stationary and automobile exhaust emission after-treatment devices (Le et al., 2024). One-dimensional ZnO nanostructure arrays grown onto commercial monolithic cordierite honeycomb as an exhaust catalyst have been introduced by P.-X. Gao et al. (Guo et al., 2013; P.-X. G. Guoz. Z. Ren, 2012). Additionally, ZnO nanorod arrays can be used as sacrificial templates for the synthesis of metal oxide nanoarrays such as ceria nanotube arrays (Safaee et al., 2019). Since ZnO nanorod arrays within the three-dimensional space of cordierite honeycomb monolith channels are typically grown by hydrothermal procedures, it is important to deposit uniform ZnO nanoseeds on the three-dimensional space of monolithic cordierite honeycomb channels in order to achieve uniformity, alignment, and high packing density of the nanorods. One of the best deposition methods for ZnO nanoseeds on a three-dimensional substrate of commercial monolithic cordierite honeycomb is the facile, cost-effective, and scalable sonochemical synthesis. So far, the exact sonochemical synthesis or chemical reaction mechanism has not been clearly understood, but the acoustic cavitation phenomenon has been proposed. Acoustic cavitation is the generation and subsequent collapse of tiny gas bubbles caused by the sonication of a solution containing the reactant. The temperature inside these bubbles can reach several thousand Kelvin (>5000 K), and the pressure can reach several hundred atmospheres (>1000 atm). Under these conditions, the solution decomposes, free radicals form, and the synthesis process begins. Device parameters such as power and frequency, and solution-related parameters such as concentration and pH, are effective in the sonochemical process. While previous studies have demonstrated ZnO deposition on cordierite honeycombs through hydrothermal methods (Kim et al., 2003; *Sonochemistry and the Acoustic Bubble*, 2015; Yasui, 2018) or physical coating techniques (Safaee et al., 2015), This work presents several key advancements: (1) The sonochemical approach achieves uniform nanoparticle deposition across the complex three-dimensional honeycomb architecture in a single step, eliminating the need for pre-treatment or seed layers required by hydrothermal growth; (2) Compared to conventional sol-gel or dip-coating methods, the process offers precise control over crystallite size (20–70 nm) and distribution through tunable sonication power and precursor concentration, addressing the common challenge of particle agglomeration; (3) The scalability and energy efficiency of this method (room-temperature process, 20-minute synthesis) surpass those of high-temperature or multi-step alternatives. To our knowledge, this is the first systematic study optimizing sonochemical parameters for ZnO nanoparticle deposition on monolithic cordierite, providing a facile, reproducible route for catalytic substrate fabrication.

In this research, ZnO nanoparticles were synthesized by a sonochemical method from a solution containing zinc acetate and ethanol and were simultaneously deposited within the three-dimensional channels of a commercial monolithic cordierite honeycomb substrate. The effects of the ultrasonic device output power and the zinc acetate precursor concentration on the distribution and size of the precipitated nanoparticles were investigated using Rietveld refinement and Scherrer equations applied to XRD and SEM data.

2. MATERIALS AND METHODS

The commercial monolithic cordierite honeycomb substrates were procured from Ir Delco Company, featuring square channels with 1 × 1 mm cross-sectional dimensions and approximately 180 μm wall thickness. Prior to deposition, the substrates were cut into uniform 1 cm^3 cubes and subjected to a rigorous cleaning procedure. This involved sequential ultrasonication in analytical-grade acetone for 15 minutes, followed by ethanol for 15 minutes, and finally deionized water for 15 minutes to ensure complete removal of both organic and inorganic contaminants. The cleaned substrates were then dried in an oven at 80°C for 2 hours.

For the sonochemical synthesis, precursor solutions were prepared by dissolving zinc acetate dihydrate ($Zn(CH_3COO)_2{\cdot}2H_2O$, ≥99% purity) in absolute ethanol to achieve three distinct concentrations: 10 mM, 20 mM, and 40 mM. The deposition process was carried out using an ultrasonic bath operating at a fixed frequency of 40 kHz with adjustable power output ranging from 100 to 400 W. In a typical procedure, the cleaned honeycomb substrates were fully immersed in 50 mL of precursor solution and subjected to sonication for precisely 20 minutes. To maintain isothermal conditions and minimize thermal effects, the reaction vessel was equipped with a water-cooling jacket that kept the solution temperature at 25 ± 2°C throughout the sonication process. All experiments were performed in triplicate under identical conditions to ensure accuracy and reproducibility. Following deposition, the samples were gently rinsed with ethanol to remove any loosely adhered particles and subsequently dried at 60°C for 1 hour.

Structural characterization was performed using a Philips X'pert diffractometer with Cu Kα radiation (λ = 1.5406 Å) operating at 40 kV and 30 mA. Two scanning protocols were employed: a standard scan covering the 2θ range from 10° to 80° with a step size of 0.02° and a scan speed of 2°/min, and a high-resolution scan focusing on the ZnO characteristic peaks (2θ = 30–37°) with an increased dwell time of 20 seconds per step and a reduced step size of 0.02° to enhance peak resolution. Crystallite size determination was carried out using both Scherrer's

equation and Rietveld refinement methods. The Scherrer analysis employed the relationship $D = 0.9\lambda/\beta\cos\theta$, where D represents crystallite size, λ is the X-ray wavelength, β denotes the full width at half maximum (FWHM), and θ is the Bragg angle. More comprehensive structural analysis was performed using Rietveld refinement implemented in Materials Studio 8.0 software, providing additional parameters including lattice constants, microstrain, and preferred orientation, while evaluating refinement quality through the profile factor (Rp) and weighted profile factor (Rwp).

Morphological examination was conducted using a TESCAN field emission scanning electron microscope operated at 5 kV accelerating voltage in secondary electron imaging mode.

Prior to SEM observation, samples were coated with a 5 nm layer of Au/Pd using a sputter coater to prevent charging effects. Multiple magnifications ranging from 5,000× to 50,000× were employed to thoroughly characterize the nanoparticle distribution and morphology across different regions of the honeycomb substrate. For quantitative analysis of particle distribution uniformity, selected SEM images were processed using ImageJ software to determine particle density per unit area. All crystallite size measurements were performed in triplicate, and results are reported as mean values accompanied by standard deviations to ensure statistical reliability.

3. RESULTS AND DISCUSSION

3.1 Effect of sonication power on the microstructural properties of ZnO

To investigate the effect of sonication power on the microstructural properties of ZnO, a solution of zinc acetate dihydrate in ethanol with a concentration of 40 mM was prepared. Cordierite honeycomb monolith pieces were then immersed in the solution, which was subjected to ultrasonic waves at a frequency of 40 kHz with power values of 100 W and 400 W. Figure 1 shows the XRD patterns of the two samples: 40 mM treated at 100 W and 40 mM treated at 400 W, obtained under standard spectrometry conditions with the normal scan speed of the device.

It can be stated that, due to the small size of the ZnO particles deposited on the surfaces of the monolithic cordierite honeycomb and their low abundance (less than 5%), no trace of ZnO phase formation was observed inside the monolith channels under normal conditions (see Figure 1).

Since the three main ZnO peaks, (100), (002), and (101), appear at angles between 30° and 37°, XRD scans of the samples in this range were performed at a reduced scan speed, with a step size of 0.02° and a dwell time of 20 seconds per step. As shown in Figure 2, both ZnO and cordierite phases can be detected in samples nucleated from a 40 mM zinc acetate solution at sonication powers of 100 W and 400 W. This demonstrates the positive effect of using optimized XRD measurement conditions on the detection of phases.

The crystallite size of the samples was calculated using Scherrer's equation, and the results are presented in Table 1. In this equation, D represents the average crystallite size, λ is the X-ray wavelength, β denotes the full width at half maximum (FWHM), and θ is the Bragg angle.

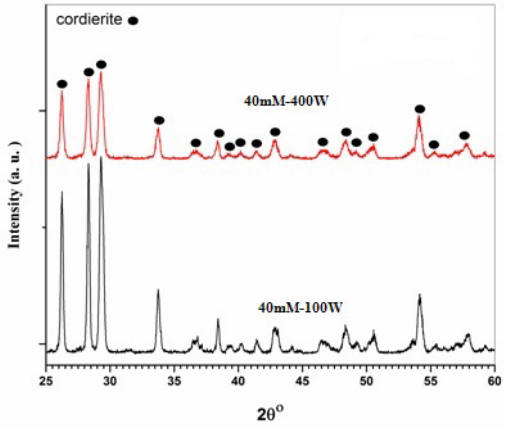

Figure 1. XRD pattern of ZnO sonochemically synthesized on the surface of monolithic cordierite honeycomb

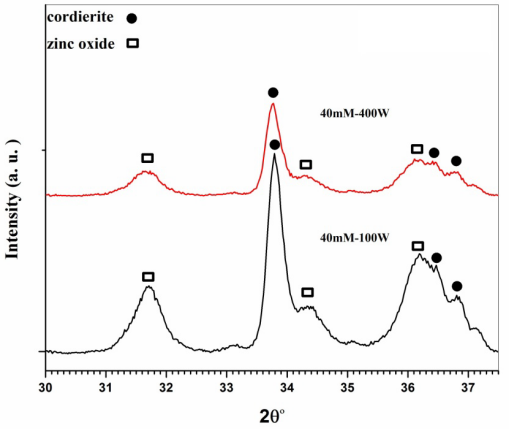

Figure 2. XRD pattern of (spectroscopy with a slow speed) of 40 mM sample at powers of 100 and 400 W

TABLE 1. The average crystallite size of the ZnO nanoparticles of 40 mM sample at powers of 100 and 400 W

Sample	Crystallite size (nm)
40 mM, 100 W	71
40 mM, 400 W	25

The results indicate that at constant zinc acetate concentration, the size of the ZnO nano crystallites decreases from 71 to 25 nanometers by increasing the sonication power. As mentioned in the experimental section, the effect of ultrasonic waves on chemical reactions and product formation has not been clearly defined yet. But the mechanism that is proposed in this method is the cavitation phenomenon, which includes:

creation, growth and collapse of bubbles in the fluid, leading to local temperatures as high as 5000 Kelvin and local pressures over 1000 atmospheres. With the growth of these bubbles to a critical size, the bubbles collapse and their stability time is about nanoseconds. Therefore, under these conditions, many chemical reactions could take place. According to the above results, it can be said that with the increase in the power of ultrasonic waves, the number of bubbles created increases for a constant amount of solution, and the difference in temperature and pressure around these bubbles becomes greater, giving rise to smaller nanoparticles.

Figure 3 shows ZnO nanoparticles well distributed within the three-dimensional channels of the monolithic cordierite honeycomb. Since the as-synthesized ZnO particles are small and the boundaries between them are indistinct, particle size cannot be determined accurately from SEM images. However, the uniform distribution of nanoparticles on the monolithic cordierite honeycomb surface (Figure 3) is evident, representing one of the most important and practical advantages of sonochemical nanoparticle synthesis.

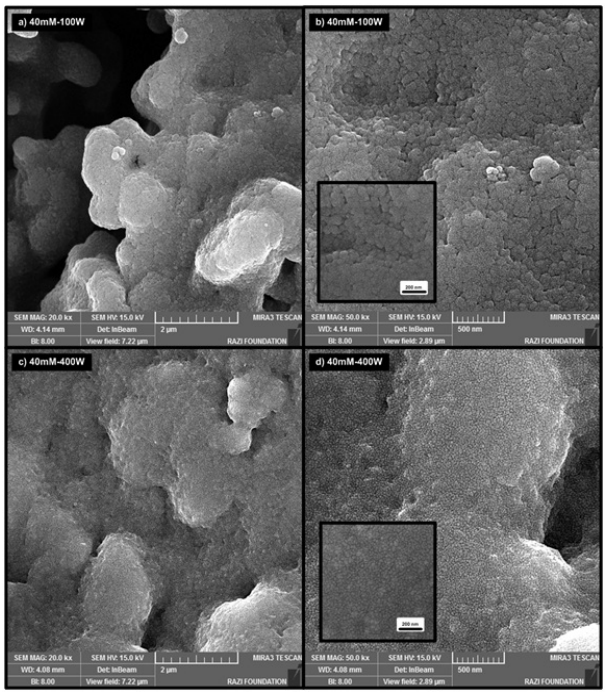

Figure 3. SEM micrographs with three magnifications for 40 mM sample at powers of 100 and 400 W

Notably, with the increase in sonication power, the 40 mM–400 W sample exhibits a more uniform distribution of ZnO nuclei compared to the 40 mM–100 W sample. Higher sonication power promotes uniform dispersion, prevents agglomeration, and improves surface area, which is critical for applications such as photocatalysis and sensing (Panigrahi et al., 2025). Conversely, low sonication power may insufficiently disrupt aggregates, resulting in larger, less uniform particles. The crystal phase, typically wurtzite for ZnO, remains stable, while higher power can enhance crystallinity by facilitating a better atomic arrangement.

From the above results, it can be concluded that increasing the sonication power applied to a solution with a constant concentration of 40 mM not only reduces the crystallite size from 71 to 25 nanometers but also enhances the uniformity of ZnO nanoparticle distribution. Therefore, a sonication power of 400 W was selected as the optimal condition.

3.2 The effect of zinc acetate concentration on the microstructural properties of ZnO

To investigate the effect of zinc acetate concentration on the microstructural properties of ZnO, solutions of zinc acetate in ethanol with concentrations of 10, 20, and 40 mM were prepared. The cordierite honeycomb monolith pieces were then immersed in the solutions, which were subjected to ultrasonic waves at a frequency of 40 kHz and a power of 400 W. According to the X-ray diffraction patterns of the samples shown in Figure 4, both ZnO and cordierite phases are observed in all three samples. In the 20 mM and 40 mM samples, all three peaks corresponding to the (100), (002), and (101) ZnO planes are clearly visible. In contrast, in the 10 mM sample, the peaks corresponding to the (101) and (002) planes are weak, due to the low concentration of the precursor solution, which results in a smaller amount of ZnO deposited on the cordierite monolith surfaces. Based on the XRD results, the average crystallite sizes of the ZnO nanoparticles were calculated using Scherrer's equation and are presented in Table 2.

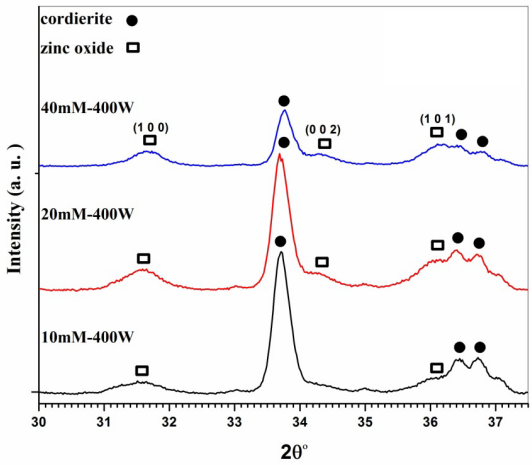

Figure 4. XRD pattern of 10, 20, 40 mM samples at sonication power of 400 W

The results in Table 2 show that at a constant sonication power, increasing the precursor concentration decreases the average crystallite size from 47 nm in the 10 mM sample to 25 nm in the 40 mM sample. As noted previously, in addition to device parameters such as the power and frequency of the applied waves, solution-

related parameters, including the type and concentration of the solute, also affect the sonochemical process. Any parameter that promotes nucleation increases the number of nuclei, which in turn reduces the size of the resulting particles. Furthermore, increasing the concentration from 10 to 40 mM raises the level of supersaturation, resulting in a larger number of nuclei and a smaller average ZnO crystallite size.

TABLE 2. The average crystallite size of the ZnO nanoparticles of 10, 20, 40 mM samples at a power rate of 400 W

Sample	Mean crystallite size
10 mM – 400 W	47
20 mM – 400 W	28
40 mM – 400 W	25

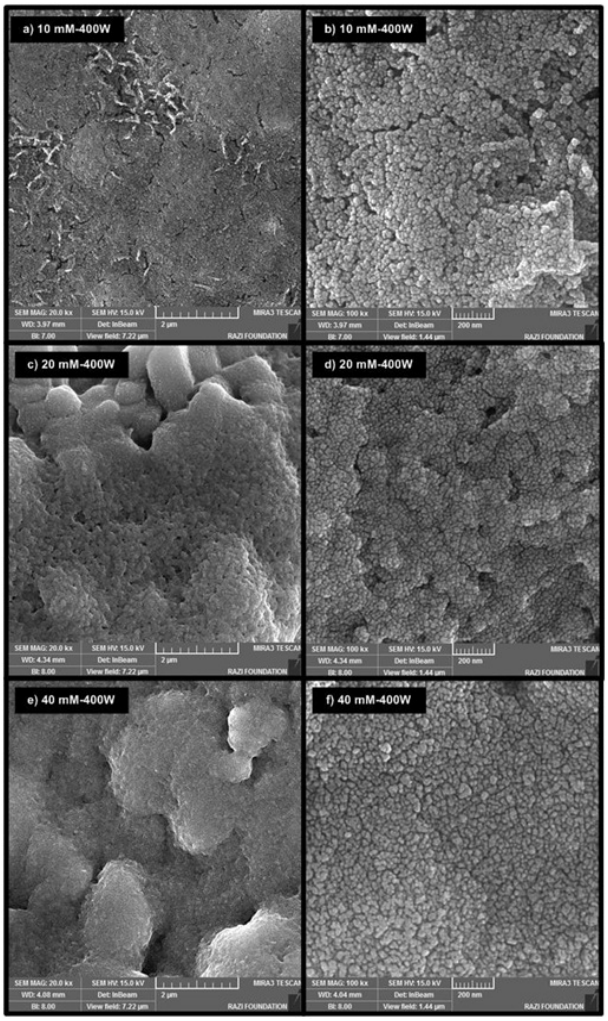

Figure 5. SEM micrographs with two magnifications for 10, 20, and 40mM samples at a sonication power rate of 400 W

To investigate the sonochemical synthesis more accurately, the Rietveld refinement method was employed to calculate crystallographic and microstructural parameters, including crystallite size, lattice constants, and microstrain. The results obtained from this method were compared with those derived from the less accurate Scherrer equation.

Figure 6 shows the refinement of the 10 mM–400 W sample using Materials Studio 8.0 software. The refinement factors Rwp and Rp, which indicate the difference between the simulated pattern generated by the software and the experimental XRD spectrum, are reported. In general, the closer these values are to zero, the more accurately the simulated pattern represents the experimental data.

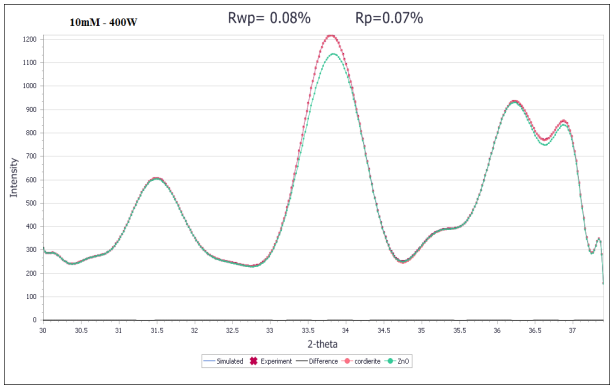

Figure 6. XRD pattern of 10mM, 400 W sample and graph simulated by the software (Materials Studio 8.0)

As shown in Figure 6, the simulated pattern generated by the software and the measured XRD pattern of the 10 mM–400 W sample are in good agreement, with only minimal differences between them. Given that the values of Rp and Rwp are close to zero, the simulation method can be used with confidence. The average crystallite sizes of the 40 mM–100 W and 40 mM–400 W samples were calculated using this method, and the results are compared with those obtained from Scherrer's equation in Table 3.

TABLE 3. Mean crystallite size of 40 mM sample at a sonication power rates of 100 and 400 W

Sample	Mean crystallite size (nm) by Scherer's method	Mean crystallite size (nm) by rietveld method
40 mM, 100W	71±2	77±2
40 mM, 400W	25±1	20±1

Based on the average crystallite sizes obtained using the Rietveld method, and considering that the X-ray diffraction measurements were performed in a specialized mode with a very low scanning speed, it can be concluded that the results obtained using Scherrer's equation are reasonably accurate, with a standard deviation of approximately 6–7 nm.

Therefore, all conclusions regarding the effect of sonication power on the average crystallite size of ZnO are confirmed with a relatively small margin of error. The

mean crystallite sizes of sonochemically synthesized ZnO nanoparticles at different zinc acetate concentrations under constant sonication power are summarized in Table 4. The discrepancy in the average crystallite size for the 10 mM–400 W sample between Scherrer's and Rietveld's methods is substantial, due to the low amount of ZnO deposited on the monolithic cordierite honeycomb surfaces, as confirmed by X-ray diffraction results. It is evident that the average crystallite size of ZnO decreases with increasing zinc acetate concentration (Table 4). As noted in the previous section, the average crystallite sizes of the 20 mM and 40 mM samples are similar. Given the acceptable uniformity in both samples and the small difference in crystallite sizes, the 20 mM sample can be considered optimal for the hydrothermal synthesis of ZnO nanoarrays.

TABLE 4. Mean crystallite sizes of 10, 20, and 40 mM samples at a sonication power rate of 400 W

Sample	mean crystallite size (nm) by Scherer's method	mean crystallite size (nm) by rietveld method
10 mM, 400 W	47±1	30±2
20 mM, 400 W	28±2	25±1
40 mM, 400 W	25±1	20±1

Comparison with similar studies shows consistency with our findings. In this study, increasing the zinc acetate concentration from 10 to 40 mM reduced the ZnO crystallite size from 47 nm to 25 nm (Scherrer's method) at 400 W sonication power, in agreement with Meroni et al. (2020), who reported smaller ZnO nanoparticles at higher precursor concentrations due to enhanced nucleation. Similarly, Panigrahi et al. (Panigrahi et al., 2025) observed improved uniformity and smaller particle sizes at higher concentrations under sonication. These results highlight the critical influence of synthesis conditions and intended applications on the microstructural properties of ZnO.

4. CONCLUSION(S)

In summary, a green and low-cost sonochemical method was employed to deposit ZnO nanoparticles uniformly onto three-dimensional cordierite honeycombs, using zinc acetate and ethanol as precursors. The effects of process and device parameters on the sonochemical synthesis were systematically investigated. First, the influence of sonication power (100 and 400 W) at a constant zinc acetate concentration of 40 mM on microstructural characteristics was examined.

Increasing the sonication power not only reduced the crystallite size from approximately 77 to 20 nm but also improved the uniformity of ZnO nanoparticle distribution. Subsequently, the effect of zinc acetate concentration on microstructural properties was studied. Increasing the zinc acetate concentration from 10 to 40 mM led to a decrease in average ZnO crystallite size from approximately 30 to 20 nm. Based on this parametric study, the optimal conditions were identified as a zinc acetate concentration of 20 mM and a sonication power of 400 W.

ACKNOWLEDGEMENTS

We sincerely thank the authorities of Imam Hossein University for their financial support, which made this research possible.

REFERENCES

1. Guo, Y., Ren, Z., Xiao, W., Liu, C., Sharma, H., Gao, H., Mhadeshwar, A., & Gao, P.-X. (2013). Robust 3-D configurated metal oxide nano-array based monolithic catalysts with ultrahigh materials usage efficiency and catalytic performance tunability. *Nano Energy*, *2*(5), 873–881. https://doi.org/10.1016/j.nanoen.2013.03.004
2. Kang, Y., Yu, F., Zhang, L., Wang, W., Chen, L., & Li, Y. (2021). Review of ZnO-based nanomaterials in gas sensors. *Solid State Ionics*, *360*, 115544. https://doi.org/10.1016/j.ssi.2020.115544
3. Kim, I.-K., Yoa, S.-J., Lee, J.-K., & Huang, C.-P. (2003). Reaction pathways and kinetic modeling for sonochemical decomposition of benzothiophene. *Korean Journal of Chemical Engineering*, *20*(6), 1045–1053. https://doi.org/10.1007/BF02706935
4. Le, H. N., Nguyen, T. B. Y., Nguyen, D. T. T., Dao, T. B. T., Nguyen, T. Do, & Ha Thuc, C. N. (2024). Sonochemical synthesis of bioinspired graphene oxide–zinc oxide hydrogel for antibacterial painting on biodegradable polylactide film. *Nanotechnology*, *35*(30), 305601. https://doi.org/10.1088/1361-6528/ad40b8
5. Liu, W., Wang, R., & Wang, N. (2010). From ZnS nanobelts to ZnO/ZnS heterostructures: Microscopy analysis and their tunable optical property. *Applied Physics Letters*, *97*(4). https://doi.org/10.1063/1.3474609
6. Magnusson, E. B., Williams, B. H., Manenti, R., Nam, M.-S., Nersisyan, A., Peterer, M. J., Ardavan, A., & Leek, P. J. (2015). Surface acoustic wave devices on bulk ZnO crystals at low temperature. *Applied Physics Letters*, *106*(6). https://doi.org/10.1063/1.4908248
7. Maleki Shahraki, M., Ali Shojaee, S., Faghihi Sani, M. A., Nemati, A., & Safaee, I. (2011). Two-step sintering of ZnO varistors. *Solid State Ionics*, *190*(1), 99–105. https://doi.org/10.1016/j.ssi.2010.06.026
8. Meroni, D., Gasparini, C., Di Michele, A., Ardizzone, S., & Bianchi, C. L. (2020). Ultrasound-assisted synthesis of ZnO photocatalysts for gas phase pollutant remediation: Role of the synthetic parameters and of promotion with WO3. *Ultrasonics Sonochemistry*, *66*, 105119. https://doi.org/10.1016/j.ultsonch.2020.105119
9. Panigrahi, U. K., Das, D., Hussain, S., Giri, J., Panda, A. K., Satapathy, P. K., & Mallick, P. (2025). Effect of sonication on the structural, optical and photocatalytic characteristics of ZnO nanostructures. *Discover Materials*, *5*(1), 82. https://doi.org/10.1007/s43939-025-00260-4
10. Ren, P.-X. G. Guoz. Z. (2012). *Metal oxide nanorod arrays on monolithic substrates* (WO2013049606A2). https://patents.google.com/patent/WO2013049606A2/en

11. Ren, X., Zhang, X., Liu, N., Wen, L., Ding, L., Ma, Z., Su, J., Li, L., Han, J., & Gao, Y. (2015). White Light-Emitting Diode From Sb-Doped p-ZnO Nanowire Arrays/n-GaN Film. *Advanced Functional Materials*, *25*(14), 2182–2188. https://doi.org/10.1002/adfm.201404316

12. Safaee, I., Kazemzad, M., Alizadeh, M., & Reza Rahimipour, M. (2015). On finding of the optimized condition for preparation of aligned ZnO nanorod arrays on monolithic cordierite honeycomb. *Ceramics International*, *41*(10), 12589–12594. https://doi.org/10.1016/j.ceramint.2015.06.077

13. Safaee, I., Kazemzad, M., Shahraki, M. M., Alipour, S., & Chermahini, M. D. (2019). Novel Ce0.8Pr0.2O2 nanotube arrays synthesized by hydrothermal method with excellent catalytic performance. *Ceramics International*, *45*(9), 11491–11494. https://doi.org/10.1016/j.ceramint.2019.03.017

14. *Sonochemistry and the Acoustic Bubble*. (2015). Elsevier. https://doi.org/10.1016/C2013-0-18886-1

15. Wang, Z. L. (2004). Zinc oxide nanostructures: growth, properties and applications. *Journal of Physics: Condensed Matter*, *16*(25), R829–R858. https://doi.org/10.1088/0953-8984/16/25/R01

16. Xie, X., Li, Y., Liu, Z.-Q., Haruta, M., & Shen, W. (2009). Low-temperature oxidation of CO catalysed by Co3O4 nanorods. *Nature*, *458*(7239), 746–749. https://doi.org/10.1038/nature07877

17. Yanagitani, T., Morisato, N., Takayanagi, S., Matsukawa, M., & Watanabe, Y. (2011). c-Axis Zig-Zag ZnO film ultrasonic transducers for designing longitudinal and shear wave resonant frequencies and modes. *IEEE Transactions on Ultrasonics, Ferroelectrics, and Frequency Control*, *58*(5), 1062–1068. https://doi.org/10.1109/TUFFC.2011.1906

18. Yang, H. G., Sun, C. H., Qiao, S. Z., Zou, J., Liu, G., Smith, S. C., Cheng, H. M., & Lu, G. Q. (2008). Anatase TiO2 single crystals with a large percentage of reactive facets. *Nature*, *453*(7195), 638–641. https://doi.org/10.1038/nature06964

19. Yasui, K. (2018). *Acoustic Cavitation and Bubble Dynamics*. Cham: Springer International Publishing. https://doi.org/10.1007/978-3-319-68237-2

20. Zhu, P., Weng, Z., Li, X., Liu, X., Wu, S., Yeung, K. W. K., Wang, X., Cui, Z., Yang, X., & Chu, P. K. (2016). Biomedical Applications of Functionalized ZnO Nanomaterials: from Biosensors to Bioimaging. *Advanced Materials Interfaces*, *3*(1). https://doi.org/10.1002/admi.201500494